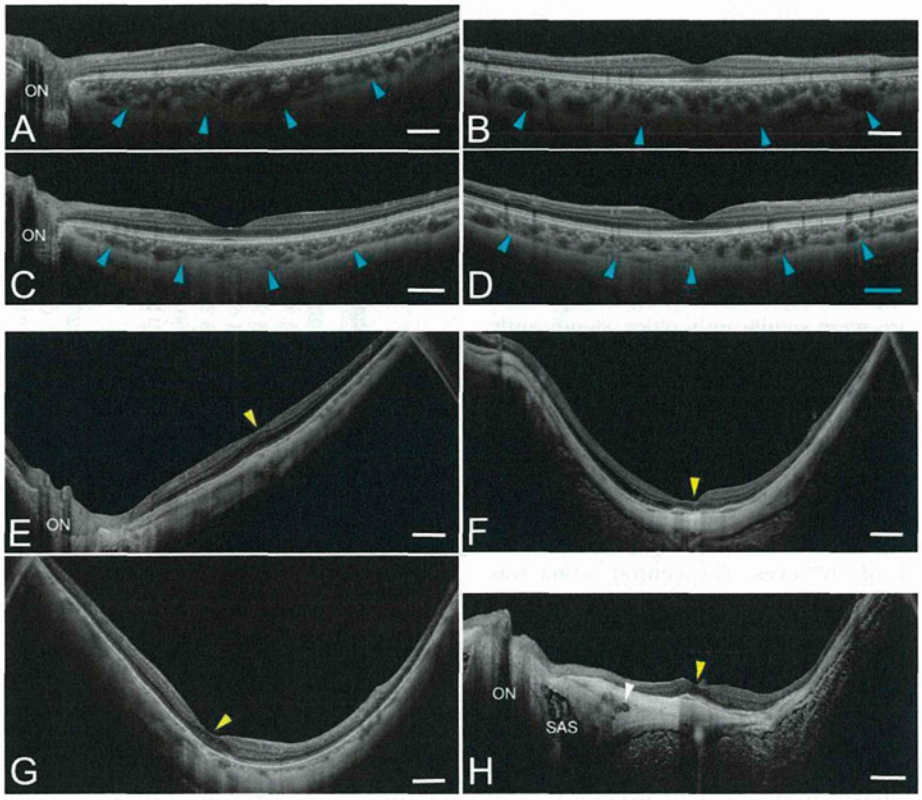

FIGURE 4. Different curvature patterns of the inner scleral surface. (**A–D**) Emmetropic eyes. In emmetropic eyes, the curve of inner scleral surface is not necessarily the same as the curve of the retinal pigmented epithelium (RPE) because a thick choroid exists between the RPE and sclera. (**A**) Horizontal scan through the central fovea shows that the RPE line is almost straight and is sloped toward the optic nerve. The curvature of the inner scleral surface (*arrowheads*) is slightly bowed and symmetric around the fovea. (**B**) Vertical scan through the central fovea of the same eye shown in (**A**) shows that the RPE line is almost straight. The curve of inner scleral surface (*arrowheads*) is slightly bowed and symmetrical around the fovea. (**C**) Horizontal scan through the central fovea shows that the RPE line is slightly bowed and the fovea is situated on the bottom of RPE curve. The curvature of the inner scleral surface (*arrowheads*) is slightly bowed and symmetrical around the fovea. (**D**) Vertical scan through the central fovea of the same eye shown in (**C**) shows that the RPE line is slightly bowed. The curvature of inner scleral surface (*arrowheads*) is slightly bowed and symmetric around the fovea. (**E–H**) Four distinct patterns of inner scleral curvature in highly myopic eyes. Due to a very thin choroid, the curvature of the inner scleral surface is almost identical to the RPE curvature, although the RPE can be atrophied in some cases. (**E**) The curvature is sloped toward the optic nerve. The curve of inner scleral surface is straight, and the optic disc is at the bottom of the posterior segment of the eye. This pattern was more obvious in horizontal than in vertical scans. The central fovea (*arrowhead*) is on the wall of the slope inclined toward the optic nerve. (**F**) The curvature is symmetrical around the fovea. The sclera is strongly bowed posteriorly; however, the curve is symmetrical around the fovea (*arrowhead*), and the fovea is situated on the bottom of posterior segment of the eye. (**G**) Asymmetrical curvature around the fovea. The sclera is strongly bowed posteriorly, and the most protruded point is away from the central fovea. The fovea (*arrowhead*) is on the slope. (**H**) Irregular curvature. The sclera is irregular and does not have a smooth curvature. The fovea is shown by the *yellow arrowhead*. Intrascleral artery is shown by *white arrowhead*. ON, optic nerve; SAS, subarachnoid space.

affected the scleral curvature. The curvature of the retinal pigment epithelium (RPE) and Bruch's membrane in emmetropic eyes had two patterns; the contour was straight and sloped toward the optic disc (Figs. 4A, 4B) or had a roughly symmetrical curvature centered on the fovea (Figs. 4C, 4D). Despite the different patterns of curvature of the RPE and Bruch's membrane, the curvature of the inner scleral surface was always symmetrical and mainly centered on the fovea.

Analysis of the contour of the inner scleral surface of 93 eyes of 75 patients with DSM and 28 eyes of 21 patients with TDS was not performed. We defined a TDS as a condition in which the upper part of the optic disc protruded anteriorly and the lower part of the optic disc sloped posteriorly in the stereoscopic fundus photographs.

In the end, the contour of the inner sclera of 367 of 488 highly myopic eyes was analyzed. The contour of the inner scleral surface had four distinct patterns (Figs. 4E–H; Table 3). The number of patients whose two eyes had different patterns was 45. The first pattern was one in which the curvature sloped toward the optic disc and the optic disc was at the bottom of the curvature (Fig. 4E). This pattern was observed in 44 of 367 eyes (12.0%) and was generally seen more clearly in horizontal than in vertical scans. In the second pattern, the curvature of the inner scleral surface was symmetrically centered on the fovea, and the fovea was situated in the center and at the bottom of the curvature (Fig. 4F). This pattern appeared to be similar to the second pattern seen in emmetropic eyes; however, the curvature appeared to be sharper than that in emmetropic controls. This type was observed in 98 of 367 eyes (26.7%). The third pattern was that in which the contour of the inner scleral surface was curved posteriorly with the curvature asymmetrical around the central fovea. The fovea was not situated at the bottom of the curvature but on the slope of the wall (Fig. 4G). This pattern was observed in 105 of 367 eyes (28.6%). The final pattern was the type in which the contour of the inner scleral surface was irregular and did not form a smooth circular arc (Figs. 4H, 5). In extreme cases, the curvature of the posterior eye segment was totally irregular (Fig. 5E). This was the most frequent pattern in eyes with pathologic myopia, one that we observed in 120 of 367 eyes (32.7%). The first pattern was significantly less frequently

observed than any other pattern ($P < 0.05$, χ^2 tests), but the differences in the incidences of the other three patterns were not significant.

Association of Clinical Characteristics of Highly Myopic Eyes with Different Types of Curvature of Posterior Segment of Eye

The clinical characteristics of highly myopic eyes with the four distinct patterns of curvature of the posterior fundus are shown in Table 3. Statistical analyses showed that the patients with irregular curvature were significantly older, significantly more myopic, and had significantly longer axial lengths than those who showed the other patterns ($P < 0.0001$, one-factor ANOVA).

A total of 66 of 367 eyes were excluded from the measurements of the central retinal thickness: 45 eyes due to myopic traction maculopathy (MTM), 18 eyes due to myopic CNV, 1 eye due to macular atrophy, and 2 eyes due to macular holes. In the end, the central retinal thickness was measured in 301 of 367 eyes. The central retina was significantly thinner in eyes with irregular curvature than in eyes with any other pattern ($P < 0.0001$, one-factor ANOVA).

The subfoveal scleral thickness was measurable in 13 of 44 eyes (29.5%) with a curve that sloped toward the optic disc, in 55 of 98 eyes (56.1%) with symmetrical curvature, in 58 of 105 eyes (55.2%) with asymmetrical curvature, and in 113 of 120 eyes (94.2%) with irregular curvature. The subfoveal sclera was thinnest in the eyes with irregular curvature, followed by the eyes with symmetrical curvature, those with asymmetrical curvature, and those with curvature toward the optic disc. A statistical comparison of the subfoveal scleral thickness among the groups was not performed because it was not possible to measure the subfoveal scleral thickness in 130 of the eyes.

The subfoveal choroid was too thin to be measured in 45 of 98 eyes (45.9%) with symmetrical curvature, in 55 of 105 eyes (52.4%) with asymmetrical curvature, in 11 of 44 eyes (25.0%) with curvature sloping toward the optic disc, and in all 120 eyes with irregular curvature. Statistical analyses showed that the number of eyes whose choroid was too thin to be measured was significantly greater among eyes with irregular curvature than in any other group ($P < 0.0001$, χ^2 tests). Also, the number of eyes whose choroid was too thin to be measured was significantly lower among eyes with curvature sloping toward the optic disc than in any other group ($P < 0.0001$, χ^2 tests).

Correlation between Curvature of Inner Scleral Surface and Myopic Fundus Lesions

In 367 of 488 highly myopic eyes in which the contour of the inner sclera was analyzed, the prevalence of a posterior staphyloma, MTM, myopic chorioretinal atrophy, and myopic CNV was 90.7% (333 eyes), 49.9% (183 eyes), 31.6% (116 eyes), and 15.3% (56 eyes), respectively. A posterior staphyloma was found in all 105 eyes with an asymmetrical curvature and in all 120 eyes with an irregular curvature (Table 3). These numbers were significantly higher than in eyes with symmetric curvature or with curvature sloping toward the optic disc ($P < 0.001$, Fisher's exact probability tests). On the other hand, a staphyloma was present in 26 of 44 eyes (59.0%) whose curvature slopped toward the optic disc, which was significantly fewer than in other groups ($P < 0.05$, Fisher's exact probability tests).

TABLE 3. Comparison of Characteristics between Highly Myopic Eyes with Different Contours of Inner Scleral Surface in Radial Scans Centered on the Fovea

	Incline toward the Optic Disc	Symmetrical, Centered on the Fovea	Asymmetrical, Fovea on the Slope	Irregular Curve	*P* Value
No. of eyes (No. of persons)	44 (30)	98 (72)	105 (75)	120 (85)	
Age, y, mean ± SD	51.3 ± 14.8 (20–74)	53.7 ± 14.1 (12–82)	56.9 ± 14.2 (12–81)	63.3 ± 10.7 (32–89)	<0.0001*
Refractive error, d, mean ± SD	−11.9 ± 3.2 (−8.5 to −20.0)	−12.9 ± 3.5 (−8.5 to −24.0)	−12.6 ± 4.5 (−8.5 to −25.5)	−16.2 ± 3.9 (−10.0 to −23.0)	<0.0001*
Axial length, mm, mean ± SD	29.2 ± 1.6 (26.6–33.4)	29.6 ± 1.9 (26.5–34.3)	29.2 ± 1.9 (26.5–36.2)	31.0 ± 1.6 (27.7–36.6)	<0.0001*
Central retinal thickness, μm, mean ± SD	178.3 ± 42.3 (95–242)	183.6 ± 28.7 (82–211)	152.0 ± 38.9 (52–253)	130.1 ± 33.2 (59–205)	<0.0001*
Subfoveal scleral thickness, μm, mean ± SD (No. of eyes whose scleral thickness was measurable)	279.7 ± 111.2 (146–477) (13)	240.9 ± 76.5 (118–528) (55)	276.4 ± 78.5 (146–546) (58)	189.1 ± 60.9 (80–380) (113)	<0.0001*
Posterior staphyloma, No. of eyes (%)					
Present	26 (59.0%)	82 (83.7%)	105 (100%)	120 (100%)	
Absent	18 (40.9%)	16 (16.3%)	0 (0%)	0 (0%)	
MTM, No. of eyes (%)	5 (11.4%)	34 (34.7%)	53 (50.5%)	91 (75.8%)	<0.0001†
Myopic chorioretinal atrophy, No. of eyes (%)	15 (11.4%)	15 (15.3%)	16 (15.2%)	70 (58.3%)	<0.0001†
Myopic CNV, No. of eyes (%)	4 (9.1%)	8 (8.2%)	11 (10.5%)	33 (27.5%)	0.004†

* One-factor ANOVA.
† χ^2 tests.

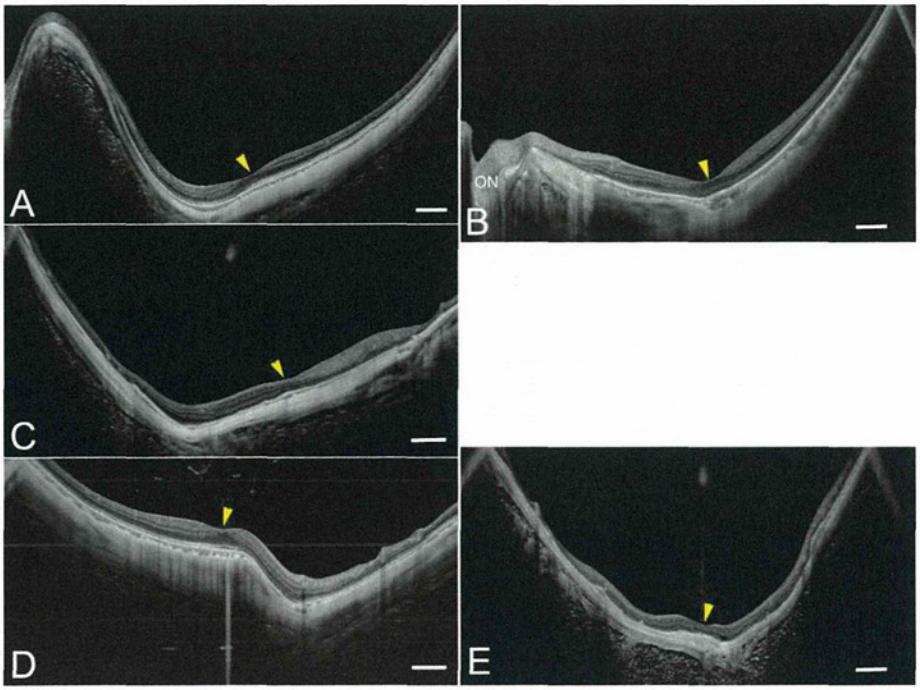

FIGURE 5. Different patterns of scleral curvature in eyes classified with irregular curvature. (**A**) The sclera nasal to the most protruded point is extremely thin and the scleral curvature is not spherical. The central fovea is on the slope (*arrowhead*). (**B**) The scleral curvature is bent at the site of the central fovea (*arrowhead*). (**C**) The scleral curvature is similar to that in (**A**); however, the curvature is more linear and the transition of the change in curvature is more acute. The central fovea is on the slope (*arrowhead*). (**D**) The scleral thickness is irregular and the sclera is acutely displaced posteriorly beside the central fovea shown by the *arrowhead*. (**E**) The sclera is extremely thin and the scleral curvature is entirely irregular. The central fovea (*arrowhead*) is almost centered in the irregular curvature.

Chorioretinal atrophy, patchy atrophy or macular atrophy, and myopic CNVs were observed significantly more frequently in eyes with irregular curvature than in any other group ($P < 0.0001$ and $P = 0.004$, respectively, χ^2 tests, Table 3). MTM was observed most frequently in eyes with irregular curvature, followed by those with asymmetrical curvature, those with symmetrical curvature, and those with a curvature that sloped toward the optic disc.

Determination of Location of Most Protruded Part of Highly Myopic Eyes with Asymmetric or Irregular Curvature

In eyes with symmetrical curvature, the central fovea sat at the bottom of the curvature of posterior segments of the eye. In eyes where the curvature sloped toward the optic disc, the optic disc was also at the bottom of the curvature.

We were able to determine the location of the most protruded part in the posterior segment in 105 eyes with asymmetric curvature and 120 eyes with irregular curvature (see Supplementary Material and Supplementary Table S1, http://www.iovs.org/lookup/suppl/doi:10.1167/iovs.12-10161/-/DcSupplemental). The most protruded point existed somewhere other than in the central fovea or optic disc in the eyes with an asymmetric curvature; the location of the most protruded part was not consistent in the eyes with irregular curvature. For our analyses, we combined the superior, temporal superior, and nasal superior into one group called the "upper" and combined the inferior, temporal inferior, and nasal inferior into one group called the "lower" (Fig. 1B). Our analyses showed that the lower area was the most protruded part both in eyes with asymmetric curve and in eyes with irregular curve (85.7% and 58.3%, respectively). In 85.7% of the eyes with asymmetric curvature, the most protruded part existed inferior to the fovea (see Supplementary Material and Supplementary Table S1, http://www.iovs.org/lookup/suppl/doi:10.1167/iovs.12-10161/-/DcSupplemental). On the other hand, the most protruded part existed in the central fovea in 28.4% of the eyes with irregular curvature. The curvature was too irregular to allow identification of the most protruded part in five eyes, and three of these eyes had macular intrachoroidal cavitation (ICC)[25] and were excluded from the analyses.

A summary of the relationship between the location of the most protruded point and the curvature of the sclera is presented in Supplementary Table S2 (see Supplementary Material and Supplementary Table S2, http://www.iovs.org/lookup/suppl/doi:10.1167/iovs.12-10161/-/DcSupplemental).

Distance and Depth of Most Protruded Part in Posterior Fundus Away from Central Fovea

The most protruded point existed away from the central fovea in all 103 eyes with asymmetrical curvature (after 2 eyes with macular ICC were excluded from the 105 eyes) and in 81 of 114 eyes with irregular curvature (after 1 eye with macular ICC and 2 eyes whose curve was too irregular for identification of the most protruded point were excluded) (see Supplementary Material and Supplementary Tables S1 and S2, http://www.iovs.org/lookup/suppl/doi:10.1167/iovs.12-10161/-/DcSupplemental). In these 184 eyes, the average distance between the most protruded part and the central fovea was 2020.1 ± 632.1 μm (772–4153 μm). The average depth of the most protruded point from the foveal plane was 251.2 ± 164.3 μm (51–978 μm). The average distance of the most protruded point from the central fovea was 2092.6 ± 675.9 μm (846–4153 μm) in the eyes with asymmetrical curvature and 1847.8 ± 565.7 μm (901–3480 μm) in eyes with irregular curvature. The most protruded point in the eyes with asymmetric curve was situated farther away from the fovea than in the eyes with

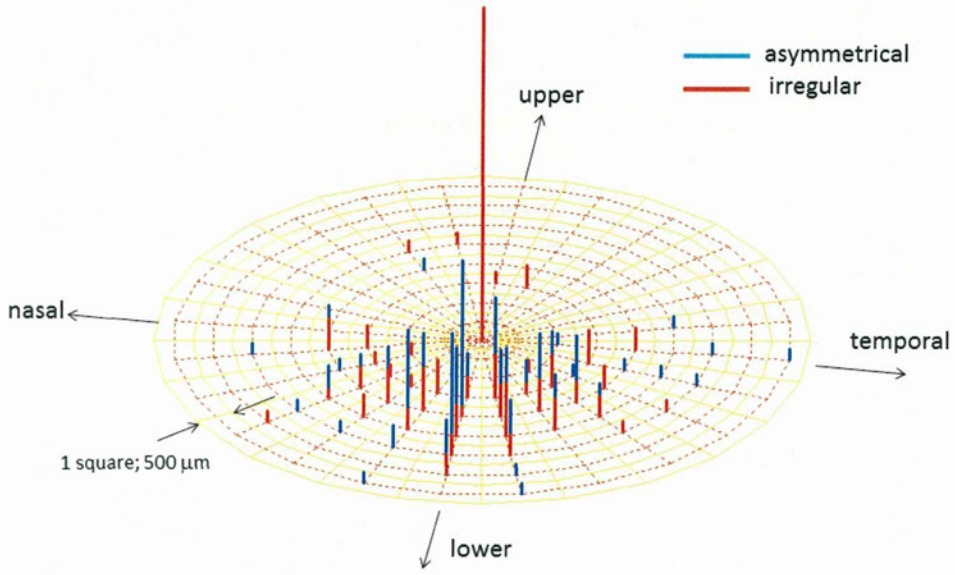

FIGURE 6. Topographic map of the distribution of the most protruded point relative to the location of central fovea in eyes with asymmetric or irregular scleral curvature. The most protruded part was identified in each of 12 radial scans centered on the central fovea, and the depth of the most protruded part from the foveal plane was measured in each scan. Then, the scan that included the most protruded part whose depth from the foveal plane was the greatest was determined. The distance of the most protruded point from the fovea was measured with the caliper function of the built-in software of swept-source OCT. The center of this graph is the central fovea. The distribution of the most protruded point is expressed on each meridian centered on the fovea according to its orientation and distance from the fovea. The *red bar* means that the eye belongs to the asymmetrical curvature group; the *blue bar* means that the eye belongs to the irregular curvature group. Each square shows 500 μm in distance.

irregular curve ($P = 0.004$, Mann-Whitney U tests). The average depth of the most protruded point from the foveal plane was 236.8 ± 155.8 μm (51–978 μm) in the eyes with asymmetrical curvature and 235.7 ± 139.5 μm (73–772 μm) in the eyes with irregular curvature. The frequency and distribution of the most protruded point in the eyes with asymmetrical curvature or with irregular curvature as a function of the distance and depth of the most protruded point from the fovea are plotted in Figure 6.

Twenty-eight highly myopic eyes with TDS were examined by swept-source OCT. To determine the difference in the curvature of the posterior segment of highly myopic eyes with and without TDS, we compared the location and depth of the most protruded part between these two groups. The clinical characteristics of the patients with TDS are shown in Supplementary Table S3 (see Supplementary Material and Supplementary Table S3 http://www.iovs.org/lookup/suppl/doi:10.1167/iovs.12-10161/-/DcSupplemental).

Among the 28 eyes with TDS, the most protruded part existed inferior to the central fovea in 21 eyes (75.0%), temporally inferior to the fovea in 4 eyes (14.3%), and nasally inferior in 3 eyes (10.7%). In the 28 eyes with TDS, the average distance of the most protruded point from the central fovea was 2992.5 ± 830.7 μm (1956–4591 μm), and the average depth of the most protruded point from the foveal plane was 673.5 ± 263.7 μm (314–1292 μm). Statistical analyses showed that the most protruded point was significantly more distant from the central fovea in the highly myopic eyes with TDS than in those without TDS ($P < 0.0001$, Mann-Whitney U tests). In addition, the depth of the most protruded point from the foveal plane was significantly greater in the eyes with TDS than in those without ($P < 0.0001$, Mann-Whitney U tests).

Scleral Thickness of Most Protruded Part Away from Central Fovea

The average scleral thickness at the most protruded part of the posterior segment was 155.8 ± 55.8 μm (52–303 μm) in all 184 eyes whose most protruded point was outside the central fovea. In eyes with asymmetric curvature, the average scleral thickness at the most protruded part was 185.2 ± 55.9 μm (96–303 μm); and in eyes with irregular curvature, it was 130.8 ± 40.0 μm (52–243 μm). Statistical analyses showed that the scleral thickness at the most protruded point was significantly less in eyes with irregular curvature than in those with asymmetric curvature ($P < 0.0001$, Welch's t-tests).

We then compared the scleral thickness at the most protruded part and the thickness at other areas. In the eyes with asymmetric curvature, the scleral thickness at the most protruded part was significantly less than the subfoveal scleral thickness and that nasal to the fovea ($P < 0.05$, Dunn's multiple comparison test). However, the differences between the thickness at the most protruded part and that temporal to the fovea or that inferior to the fovea were not significant. In the eyes with irregular curvature, the scleral thickness at the most protruded part was significantly less than the thickness of the subfoveal sclera, that nasal to the fovea, and that superior to the fovea ($P < 0.05$, Dunn's multiple comparison test). However, the differences in the thickness between the most protruded part and that temporal to the fovea or between the most protruded part and that inferior to the fovea were not significant.

Correlation between Shape of Globe Determined by 3D MRI and Contour of Inner Scleral Surface Determined by OCT

Forty-three patients (70 eyes) agreed to undergo a 3D MRI examination according to the protocol we reported previously.[11] Written informed consent was obtained from each patient for the 3D MRI examination. The results are summarized in Table 4. The degree of symmetry of the posterior eye segment in the horizontal and sagittal planes, as well as the pointedness of the posterior pole of the eye, was analyzed in the 3D MRIs (Fig. 2). Although statistical analyses were not performed due to the limited number of

TABLE 4. Correlation between Eye Shape Examined by 3D MRI and Curvature of the Posterior Segment of the Eye by OCT

3D MRI Analyses*	Incline toward the Optic Disc (5 eyes)	Symmetrical, Centered on the Fovea (16 eyes)	Asymmetrical, Fovea on the Slope (24 eyes)	Irregular Curve (25 eyes)
Symmetricity in horizontal plane				
Symmetrical	0 eyes (0%)	16 eyes (100%)	21 eyes (87.5%)	16 eyes (64.0%)
Nasally distorted	5 eyes (100%)	0 eyes (0%)	3 eyes (12.5%)	7 eyes (28.0%)
Temporally distorted	0 eyes (0%)	0 eyes (0%)	0 eyes (0%)	2 eyes (8.0%)
Symmetricity in sagittal plane				
Symmetrical	2 eyes (40.0%)	12 eyes (75.0%)	11 eyes (45.8%)	13 eyes (52.0%)
Inferiorly distorted	3 eyes (60.0%)	3 eyes (18.8%)	14 eyes (58.3%)	12 eyes (48.0%)
Superiorly distorted	0 eyes (0%)	1 eye (6.3%)	0 eyes (0%)	0 eyes (0%)
Sharpness of posterior segment of the eye				
Pointed	2 eyes (40.0%)	2 eyes (12.5%)	10 eyes (41.7%)	18 eyes (72.0%)
Dull	3 eyes (60.0%)	14 eyes (87.5%)	14 eyes (58.3%)	7 eyes (28.0%)

* See Methods for details.

eyes analyzed by 3D MRI, there was some tendency for the shape as determined by 3D MRI to fall into the four distinct patterns of curve of the inner scleral surface. Among the eyes with scleral curvature inclined toward the optic disc, all were not horizontally symmetrical and all were the nasally distorted type. Among the eyes with symmetrical curvature, all were horizontally symmetrical and 75% were sagittally symmetrical as well. Among eyes with asymmetric curvature, horizontal symmetry was found in 87.5%; however, the number of eyes with sagittal symmetry decreased to 45.8%, and 58.3% of the eyes had the inferiorly distorted shape. Among eyes with irregular curvature, horizontal symmetry was observed in 64.0%, and the temporally distorted type was identified only in this group.

Regarding the sharpness of the posterior segment of the eyes, the pointed shape was observed significantly more

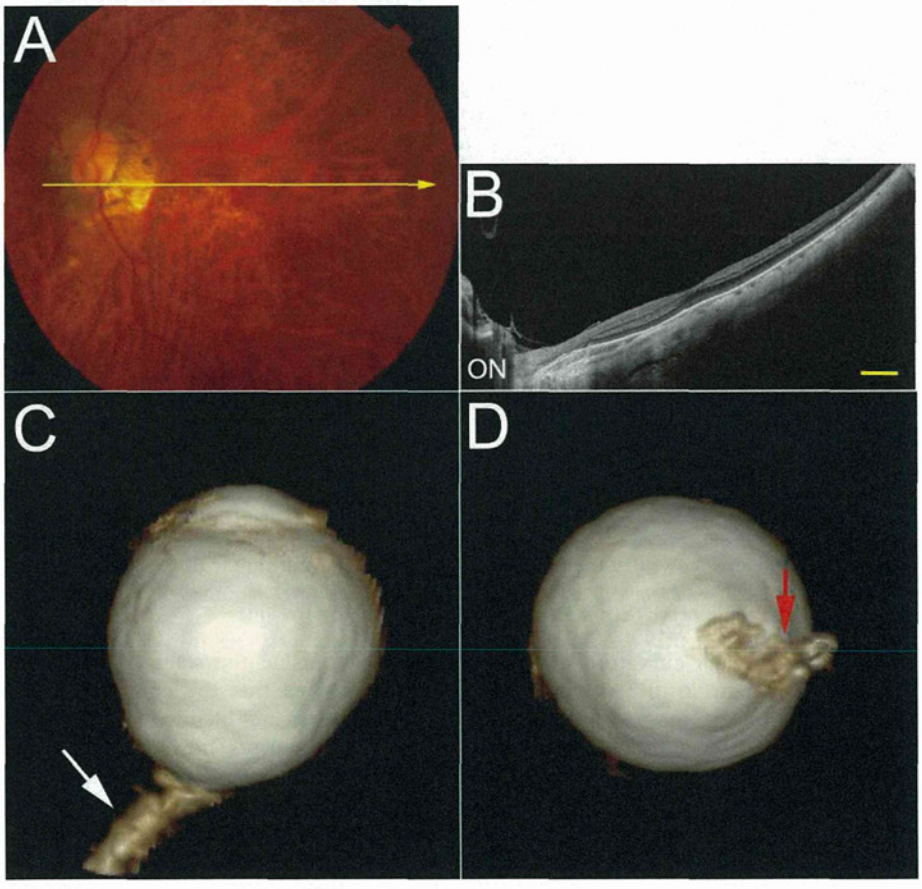

FIGURE 7. Relationship between highly myopic eyes with the scleral curvature sloped toward the optic nerve by OCT and nasally distorted eye by 3D MRI. (**A**) Left fundus of a 71-year-old woman with myopic refractive error of −9.5 diopters and an axial length of 26.6 mm. The fundus photograph shows a ring conus around the optic disc and mild chorioretinal atrophy in the macula. *Yellow line* shows a scanned line by OCT in (**B**). (**B**) Image from a horizontal OCT scan shows that the retinal pigment epithelium (RPE) and the curvature of the inner scleral surface are almost straight and are sloped toward the optic nerve (ON). *Scale bar* = 1 mm. (**C**) Inferior view of a 3D MRI image of the eye shows that the globe is elongated slightly nasally and that the optic nerve (*arrow*) is attached at the most protruded part of the globe. (**D**) Posterior view of 3D MRI image of the eye shows that the optic nerve (*arrow*) is attached at the center of the protrusion of the globe.

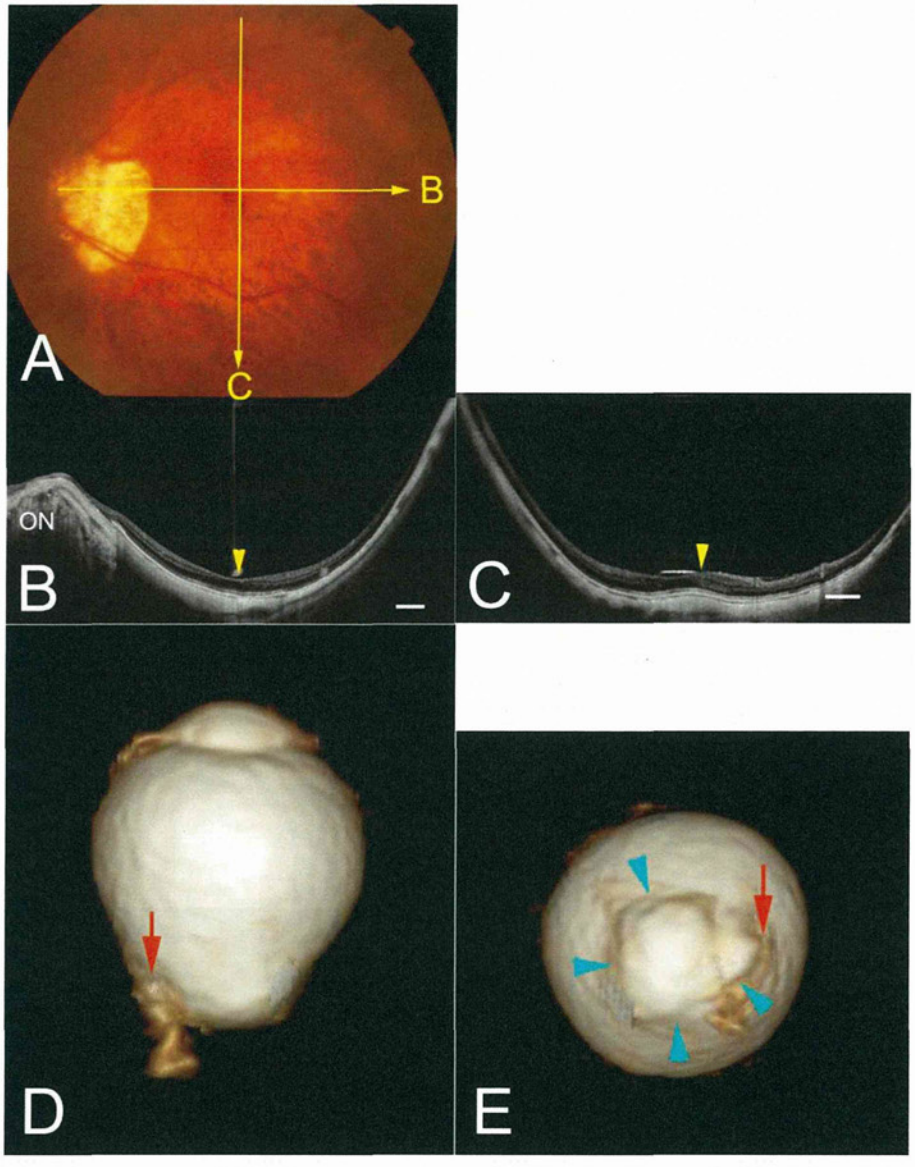

FIGURE 8. OCT image of highly myopic eye with a symmetrical curvature of the sclera centered on the fovea, and 3D MRI image of the same eye showing symmetrical elongation both horizontally and sagittally. (**A**) Photograph of the fundus of the left eye of a 70-year-old man with myopic refractive error of −15.0 diopters and an axial length of 29.5 mm. Photograph shows a temporal conus with a marked tilting of the optic disc. Mild chorioretinal atrophy is seen in the macula. *Yellow lines* show scanned lines by OCT in (**B**) and (**C**). (**B**, **C**) Horizontal (**B**) and vertical (**C**) scans showing that the curvature of the inner scleral surface is symmetrical around the central fovea (*arrowhead*). ON, optic nerve. *Scale bar* = 1 mm. (**D**) Inferior view of 3D MRI image of the eye shows that the globe is elongated symmetrically in the horizontal plane. The optic nerve (*arrow*) is attached nasal to the protrusion of the globe. (**E**) Posterior view of 3D MRI image of the eye shows that the protrusion (*arrowheads*) is almost centered horizontally and vertically. The optic nerve (*arrow*) is attached nasal to the protrusion.

frequently (75.0%) in eyes with irregular curvature whereas the dull shape was always dominant in the other three groups.

Representative cases with the four different types of curvatures of the inner scleral surface are shown in Figures 7 through 10.

DISCUSSION

Examinations of highly myopic eyes by swept-source OCT showed that the entire layer of the sclera appeared as a uniform hyperreflective structure. The outer boundary of the sclera was clearly seen in 57% of 488 highly myopic eyes. In some cases, even Tenon's capsule and the episclera, which is composed of irregularly arranged collagen fibers,[30] were observed outside the sclera. The swept-source OCT images clearly showed that the connective tissue fibers of Tenon's capsule spread and blended into the orbital fat posteriorly.

Statistical analyses showed that many factors, for example age, axial length, staphyloma, central retinal thickness, and thinness of the choroid, were significantly correlated with the visibility of the entire scleral layer. Multiple regression analyses were not performed because the objective variable, the visibility of entire layer of sclera, was not a continuous variable. Thus, we could not determine which factors affected the visibility of the outer border of the sclera most significantly. In addition, it is possible that some of these factors might be correlated with each other as reported in part by Fujiwara et al.,[31] who found a significant correlation between macular choroidal thickness and age and refractive error. It is likely that an increase in age and axial length causes a decrease

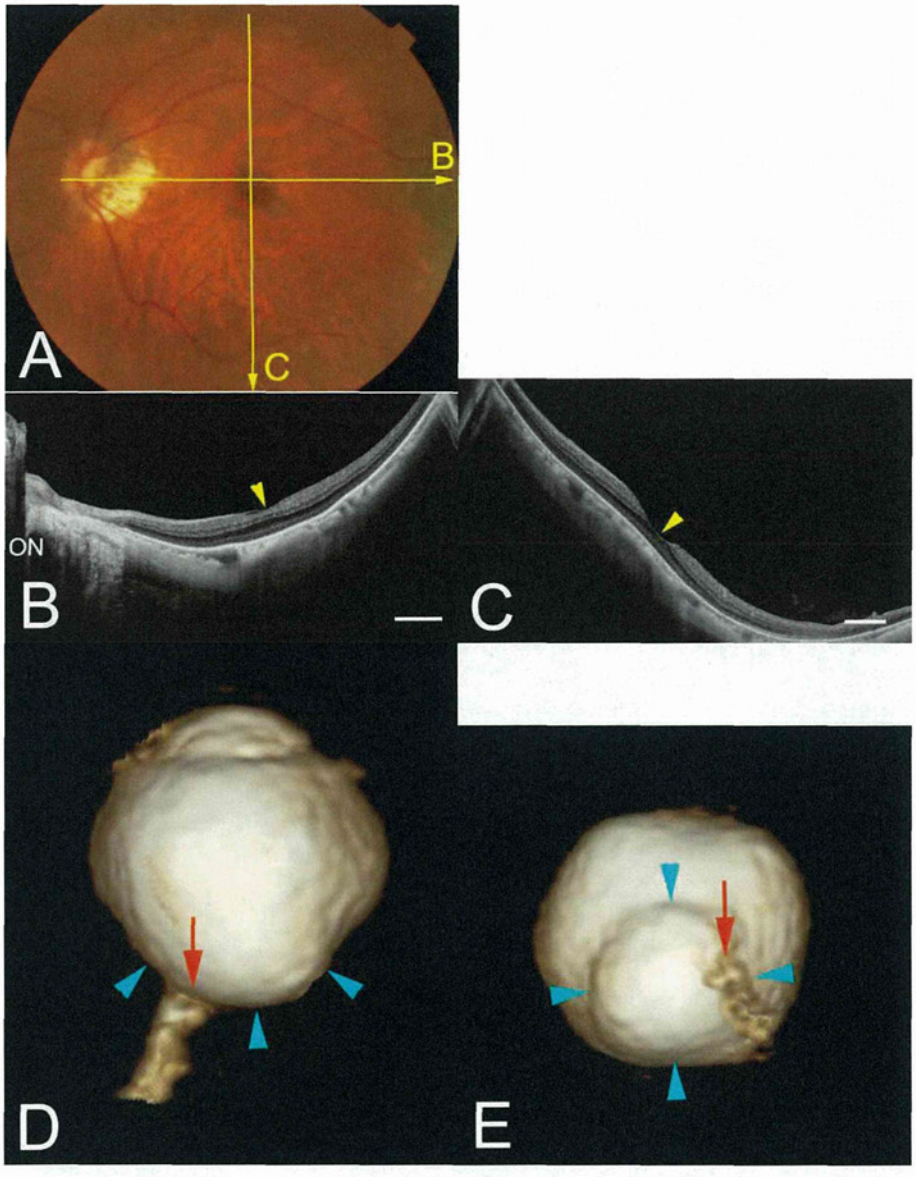

FIGURE 9. OCT image of a highly myopic eye with asymmetrical curvature of the sclera and 3D MRI image of the same eye showing an inferiorly distorted eye. (**A**) Photograph of the left fundus of a 68-year-old woman with an axial length of 28.2 mm (intraocular lens–implanted eye) showing a temporal conus around the optic disc. *Yellow lines* show scanned lines by OCT in (**B**) and (**C**). (**B**) Horizontal OCT scan showing that the most protruded point is slightly nasal to the central fovea (*arrowhead*). ON, optic nerve. *Scale bar* = 1 mm. (**C**) Vertical OCT scan showing that the most protruded point is inferior to the central fovea. The fovea (*arrowhead*) is on the slope. *Scale bar* = 1 mm. (**D**) Inferior view of 3D MRI image of the eye shows that the globe is elongated symmetrically in the horizontal plane. The optic nerve (*arrow*) is situated within the protrusion shown by the arrowheads. (**E**) Posterior view of 3D MRI image of the eye shows that the protrusion (*arrowheads*) is located inferiorly. The optic nerve (*arrow*) is located within the nasal margin of the protrusion.

in thickness of the retina and choroid in the area of a posterior staphyloma, and this could affect the visibility of entire scleral layer.

Our results showed that the average subfoveal scleral thickness in 278 highly myopic eyes without a DSM was 228 μm. Curtin[14] used histological studies to show that the scleral thickness at the posterior pole of normal eyes with axial lengths between 22 and 24 mm was 660 μm, whereas it was 233 μm in myopic eyes with an axial length of 27.8 mm. A PubMed search identified only one article whose authors had measured the scleral thickness in highly myopic eyes.[21] Imamura et al.[21] used EDI-OCT to show that the mean subfoveal scleral thickness in 25 highly myopic eyes without a DSM and a mean refractive error of −11.7 ± 5.5 D was 281 ± 85 μm. The values measured histologically[9] and by EDI-OCT[21] are comparable to the values we found.

The measurement of scleral thickness in different areas showed that the sclera was thickest 3000 μm nasal to the central fovea, followed by the subfoveal area and then by the areas temporal, superior, and inferior to the fovea. In 29 eyes with type IX staphyloma, the sclera 3000 μm nasal to the fovea was too thick to measure because of the scleral ridge that is characteristic of type IX staphyloma.[12,29] Imamura et al.[21] reported that the average scleral thickness 3000 μm temporal to the fovea was 320 μm in highly myopic eyes without DSM; this was greater than the subfoveal scleral thickness (281 μm) in the same patients. The reason for the discrepancy between their results and ours was not determined; however, one possibility might be that we studied more severely myopic eyes with irregular curvature of sclera. Our results suggested the possibility that in highly myopic eyes without evidence of

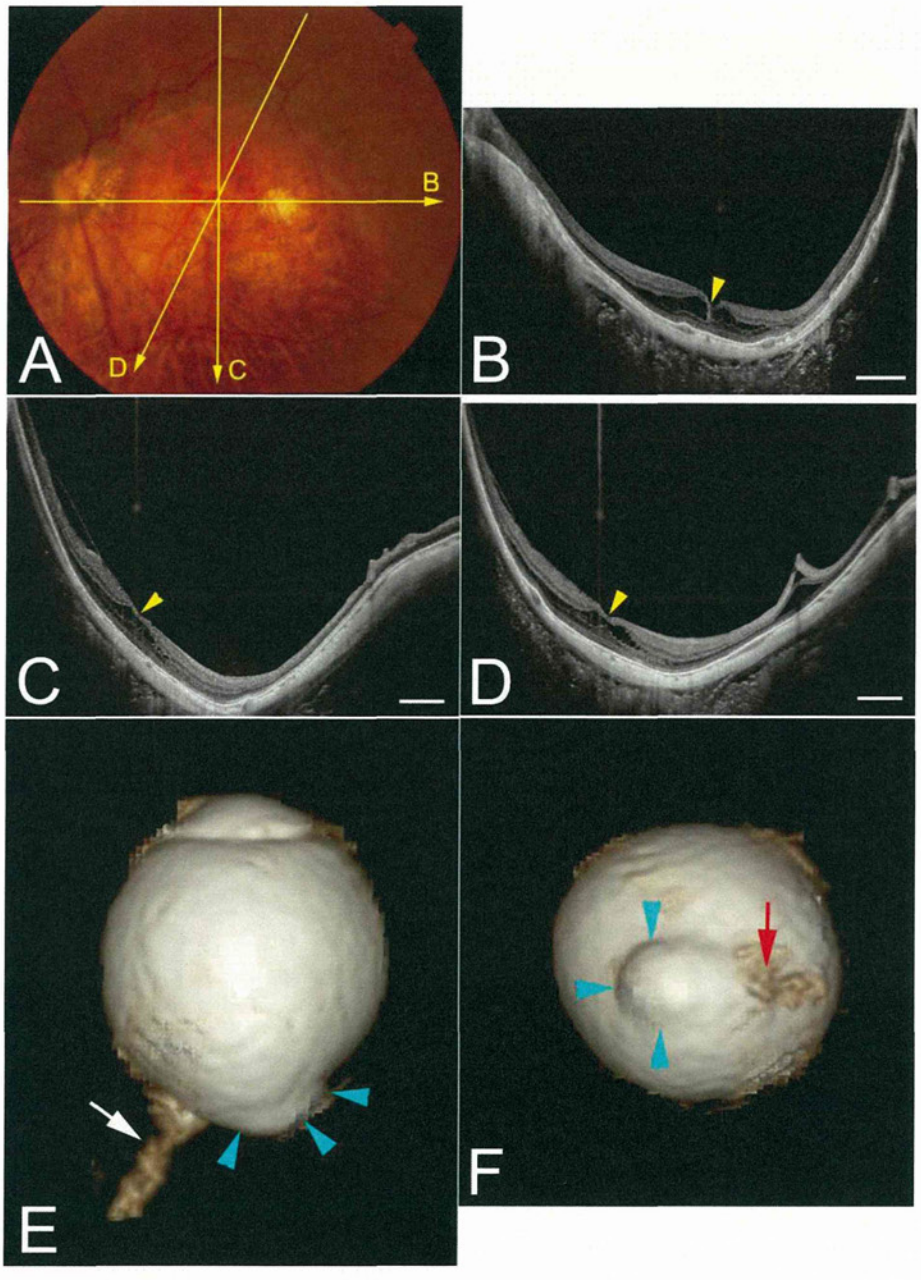

Figure 10. OCT image of a highly myopic eye with irregular curvature of the sclera and 3D MRI image showing temporally distorted eye. (**A**) Photograph of the left fundus of a 74-year-old woman with an axial length of 32.4 mm (intraocular lens–implanted eye) showing severe chorioretinal atrophy in the macula. *Yellow lines* show scanned lines by OCT in (**B**), (**C**), and (**D**). (**B**) Horizontal OCT image showing that the sclera is thin and is not spherical. The orbital fat tissue is clearly seen posterior to the sclera. Macular retinoschisis is seen around the central fovea (*arrowhead*). *Scale bar* = 1 mm. (**C**, **D**) OCT image from a vertical scan (**C**) and image from an oblique scan (**D**). The scleral contour is not spherical, and the most protruded point is located inferior to the central fovea (*arrowhead*). Macular retinoschisis can also be seen. *Scale bars* = 1 mm. (**E**) Inferior view of 3D MRI image of the eye shows that the posterior segment of the globe is temporally dislocated. The optic nerve (*arrow*) is attached nasal to the protrusion (*arrowheads*) of the globe. (**F**) Posterior view of 3D MRI image of the eye shows that the optic nerve (*arrow*) is attached nasal to the protrusion (surrounded by *arrowheads*).

DSM, the subfoveal sclera is thicker than the sclera temporal, inferior, and superior to the fovea. This needs to be confirmed in a larger population including persons with less myopic eyes.

While the curvature of the RPE and Bruch's membrane had two distinct patterns in emmetropic eyes (Figs. 4A–D), the curvature of the inner scleral surface was consistently symmetrical around the central fovea. On the other hand, the curvature of the inner scleral surface was almost identical to that of the RPE and Bruch's membrane in highly myopic eyes, mainly due to a very thin choroid situated between Bruch's membrane and the sclera.

In highly myopic eyes, the curvature of the inner scleral surface in the posterior segment of the eye had four distinct patterns: symmetrical around the central fovea, sloping toward the optic disc, asymmetrical around the fovea, and irregular curvature. The first two patterns appeared to be similar to the contour of the RPE and Bruch's membrane in emmetropic eyes, although the degree of curvature was greater in the highly myopic eyes. These findings suggested the possibility that the symmetrical shape around the fovea and sloping toward the optic disc might be an exaggerated form of the

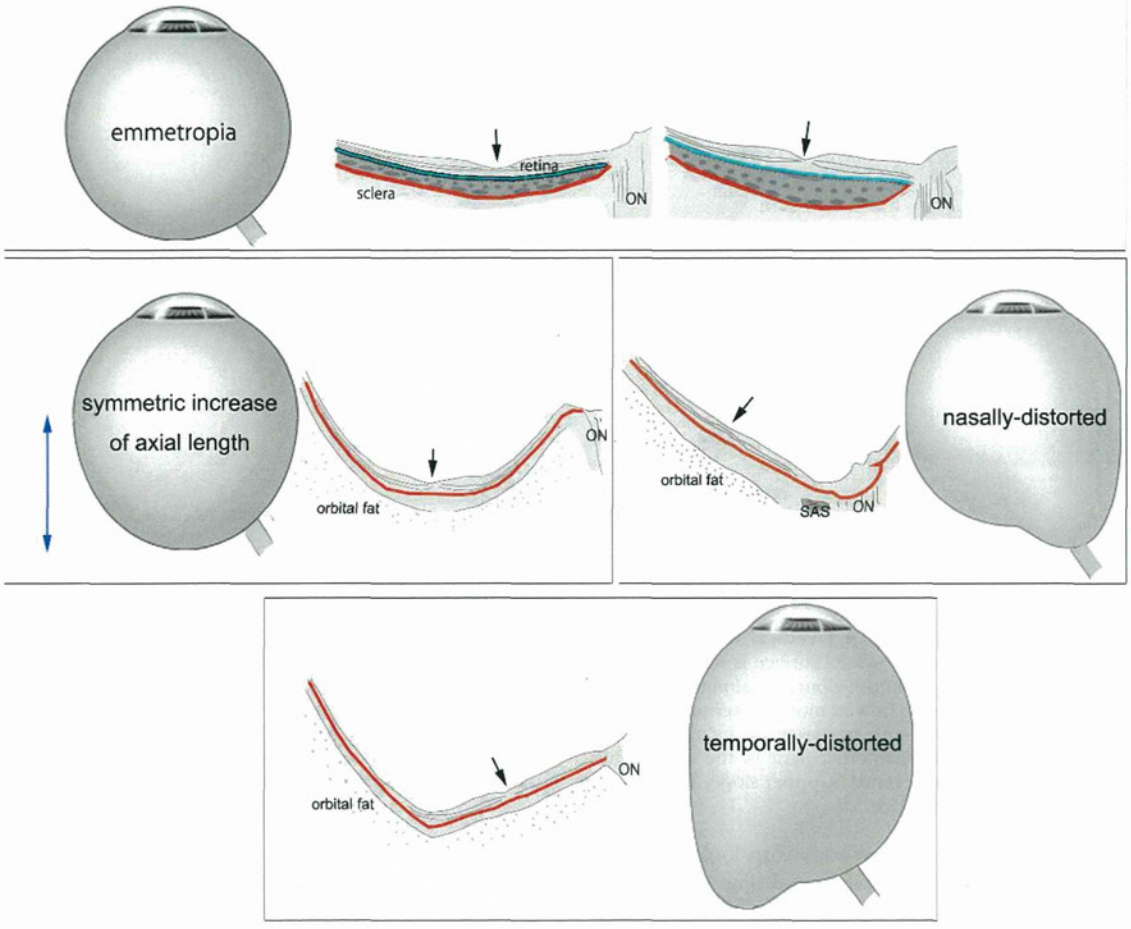

Figure 11. Schematic illustration of our hypothesis on how eye deformities in the horizontal plane progress in pathologic myopia, based on 3D MRI image and the results obtained by swept-source OCT. *Top row*: Emmetropic eyes. There are two different curvature patterns of the RPE and Bruch's membrane (shown as *blue line*) in emmetropic eyes: straight sloping of the sclera toward the optic nerve and mildly bowed centered on the fovea. However, the curvature of the inner scleral surface (*red line*) is mildly bowed posteriorly and always symmetrical around the fovea. This is due to the thick choroid affecting the curvature of the inner scleral surface in emmetropic eyes. *Middle row, left*: Symmetrically elongated highly myopic eye. When the eye elongates around the fovea, the symmetric curve of sclera seen in emmetropic eyes is exaggerated. The central fovea is on the most protruded point of the sclera. *Middle row, right*: Nasally dislocated eye in high myopia. When the eye elongated toward the optic nerve, the curvature of the inner scleral surface had an exaggeration of the RPE and Bruch's membrane slope as seen in the *top row, right* figure. The curvature of the inner scleral surface is almost straight and sloped toward the optic nerve. *Bottom row*: Temporally dislocated eye in high myopia. When the sclera thins and expands further in extremely myopic eyes, the very thin sclera can no longer maintain the curvature, and an irregular curvature results as seen in the OCT image. The area temporal to the central fovea appears to expand more and shows a temporally dislocated type by 3D MRI of the globe. The curvature of the inner scleral surface is shown as a *red line*, and the central fovea is shown by an *arrowhead* in each image. ON, optic nerve; SAS, subarachnoid space.

normal curvature of the RPE and Bruch's membrane seen in emmetropic eyes. In highly myopic eyes with very thin choroid, the scleral curvature was almost identical to the RPE curve. We suggest that when an eye elongates without forming a staphyloma, the patterns may be the same as seen in emmetropic eyes but more exaggerated in highly myopic eyes.

On the other hand, the asymmetrical and irregular patterns were observed only in highly myopic eyes. In the eyes with asymmetrical curvature around the central fovea, the most protruded point was almost always present inferiorly, including temporally inferior and nasally inferior to the fovea (see Supplementary Material and Supplementary Table S1, http://www.iovs.org/lookup/suppl/doi:10.1167/iovs.12-10161/-/DcSupplemental; Fig. 6). The fovea in these eyes was located on the superior slope of the curvature. All of the eyes with asymmetrical curvature had a staphyloma that was seen significantly more frequently than in eyes with symmetrical curvature or curvature sloping toward the optic disc. We have reported that the most protruded part of the eye existed along the visual axis in 78% of the highly myopic eyes, and inferior to the central axis in 22% of the eyes in the 3D MRI images.[11] These findings indicate that the inferior sclera expands more in highly myopic eyes. The sclera in the lower half of the eye is the area where the embryonic ocular fissure closes, and thus it might be possible that this part of the sclera is structurally weaker than the other areas. This also suggests some similarities between pathologic myopia and TDS, although the posterior bulge existed more peripherally in the inferior fundus and the degree of bulge was greater in eyes with TDS than in highly myopic eyes without evidence of the TDS. During the development of a staphyloma, the greater expansion of the inferior sclera compared to other parts of the sclera might cause a shift of the most protruded part from the subfovea to the inferior fundus, and in turn the fovea might be shifted onto the upper slope of the sclera (Fig. 11).

In the eyes with irregular curvature of the sclera, the most protruded point existed in the fovea in 28% and in the inferior fundus in 58% of the eyes (see Supplementary Material and

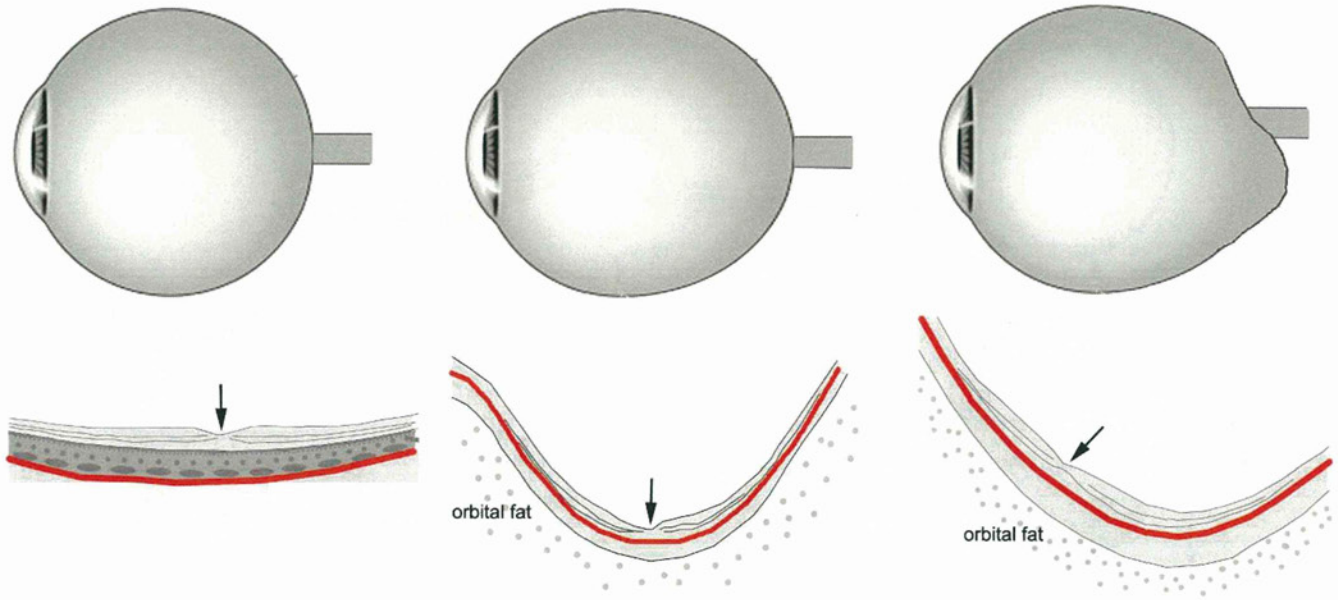

FIGURE 12. Schematic illustrations of our hypothesis on how eye deformities in the sagittal plane progress in pathologic myopia based on 3D MRI images and the images of swept-source OCT vertical scans. *Left*: Emmetropic eye. The globe is spherical by 3D MRI, and the vertical OCT scan shows that the curvature of the inner scleral surface is mildly bowed and symmetrical around the central fovea. *Middle*: Symmetrically elongated highly myopic eye. When the eye simply elongates along the central axis, the symmetrical curvature of the sclera seen in emmetropic eyes is exaggerated. The scleral curvature is bowed more posteriorly, and the central fovea is on the most protruded point of the sclera. *Right*: Inferiorly distorted eye with high myopia. When a posterior staphyloma develops in later life, the posterior sclera is expanded nonuniformly, and the lower sclera tends to be expanded more than other parts of the sclera. This causes a shift of the most protruded point from the subfovea to the lower fundus, and the fovea tends to move onto the upper slope. The curvature of the inner scleral surface is shown as a *red line*, and the central fovea is shown by an *arrowhead* in each image.

Supplementary Table S1, http://www.iovs.org/lookup/suppl/doi:10.1167/iovs.12-10161/-/DcSupplemental; Fig. 6). The patients whose eyes had an irregular curvature were significantly older; and their eyes were more myopic, had longer axial lengths, and had thinner central retinal thickness than any of the other types (Table 3). Also, the subfoveal sclera was significantly thinner, as thin as 189 μm, in the eyes with irregular curvature compared to other groups.

The myopic fundus lesions, for example, chorioretinal atrophy, CNV, and MTM, were observed significantly more frequently in eyes with irregular curvature than in those with any other type of scleral curvature. We suggest that when the sclera is stretched and becomes extremely thin, it can no longer maintain its normal curvature, and this would contribute to the development of myopic fundus lesions. Thus, irregular curvature might be the most severe and advanced form of pathologic myopia.

Finally, we compared the shape of the eye determined by 3D MRI and the contour of the inner scleral surface determined by OCT (Table 4, Figs. 7–10). The results showed that all the eyes with a curvature sloping toward the optic disc by OCT were nasally distorted as evidenced by MRI according to our definition[11] (Table 4, Fig. 7). Seventy-five percent of the eyes with symmetrical curvature by OCT were also symmetrical horizontally and sagittally in the MRI images (Table 4, Fig. 8). Horizontal symmetry was less frequent in eyes with irregular curvature (Table 4), and the temporally distorted type was observed only in eyes with irregular curvature. We have reported that significant visual field defects[7] not explained by myopic fundus lesions were observed significantly more frequently in temporally distorted eyes than in other types (nasally distorted, cylinder, or barrel type).[11] Also, among eyes with irregular curvature, those with a pointed posterior pole were observed more frequently than those with the dull shape. We recently found that the posterior pole of highly myopic eyes becomes more pointed as patients age (unpublished data). Probably the development and increase in depth of the staphylomas are the cause for the increased pointedness.

When the results of 3D MRI analyses and OCT findings are combined, the temporally dislocated types might represent a condition in which the sclera is extremely thinned and becomes irregular in contour at an advanced stage of pathologic myopia with a deep staphyloma. In fact, 46% of the eyes with asymmetrical curvature were judged to be symmetrical in both the horizontal and sagittal planes by 3D MRI. These findings suggest a possibility that swept-source OCT might be able to detect more minute and subtle deformities of the posterior segments of the eye than MRI, although the scanned area is limited. It would be the best to use both swept-source OCT and 3D MRI to analyze the shape of the globe.

Schematic illustrations of our hypothesis on how the eye deformities progress in pathologic myopia, based on the 3D MRI findings in our earlier study[11] and the swept-source OCT results in this study, are shown in Figures 11 and 12. Despite the two different curvatures of the RPE and Bruch's membrane in emmetropic eyes, the curvature of the inner scleral surface was mildly bowed posteriorly and consistently symmetrical around the fovea (Fig. 12, top row). When the eye simply elongates around the fovea or elongates toward the optic nerve, the curvature of the inner scleral surface as well as the curvature of Bruch's membrane in highly myopic eyes had an exaggeration of the patterns of the RPE and Bruch's membrane curvature seen in emmetropic eyes (Fig. 12, middle row).

When a posterior staphyloma develops in later life, the posterior sclera is expanded in a nonuniform fashion, and the lower sclera tends to expand more than other parts of the sclera (Fig. 11, right). This causes a shift of the most protruded point from the subfovea to the inferior fundus, and the fovea tends to move onto the superior slope. When the sclera thins and expands further in extremely myopic eyes, the very thin sclera can no longer maintain the curvature, and this results in

an irregular curvature (Fig. 12, bottom row). A long-term study on the course of deformation of eyes with pathologic myopia is necessary to support our hypothesis.

There are several limitations to this study. The study was conducted in the High Myopia Clinic at our university. Thus, the results might not reflect the tendency in the general myopic population. Also, 3D MRI analyses were performed in a limited number of patients who agreed to the MRI examination. Thus, the data obtained through comparison of the 3D MRI and OCT images might not apply to the rest of our highly myopic patients. Also, eyes with DSM were excluded from the analyses of scleral curvature.

Despite all of these limitations, we believe that our results obtained by swept-source OCT provide important information on the in situ shape of the sclera and the differences in the scleral curvature in highly myopic eyes. We conclude that swept-source OCT is a powerful tool to examine deeper tissues of the eye in situ, and use of this tool can provide information on how specific patterns of scleral curvatures could damage the macula and optic nerve, which can then lead to the vision-threatening complications in pathologic myopia.

Acknowledgments

The authors thank Duco Hamasaki for his critical discussion and final manuscript revision.

References

1. Green JS, Bear JC, Johnson GJ. The burden of genetically determined eye disease. *Br J Ophthalmol.* 1986;70:696-699.
2. Krumpaszky HG, Ludtke R, Mickler A, Klauss V, Selbmann HK. Blindness incidence in Germany. A population-based study from Wurttemberg-Hohenzollern. *Ophthalmologica.* 1999; 213:176-182.
3. Munier A, Gunning T, Kenny D, O'Keefe M. Causes of blindness in the adult population of the Republic of Ireland. *Br J Ophthalmol.* 1998;82:630-633.
4. Cotter SA, Varma R, Ying-Lai M, Azen SP, Klein R. Causes of low vision and blindness in adult Latinos: the Los Angeles Latino Eye Study. *Ophthalmology.* 2006;113:1574-1582.
5. Buch H, Vinding T, La Cour M, Appleyard M, Jensen GB, Nielsen NV. Prevalence and causes of visual impairment and blindness among 9980 Scandinavian adults: the Copenhagen City Eye Study. *Ophthalmology.* 2004;111:53-61.
6. Iwase A, Araie M, Tomidokoro A, Yamamoto T, Shimizu H, Kitazawa Y. Prevalence and causes of low vision and blindness in a Japanese adult population: the Tajimi Study. *Ophthalmology.* 2006;113:1354-1362.
7. Ohno-Matsui K, Shimada N, Yasuzumi K, et al. Long-term development of significant visual field defects in highly myopic eyes. *Am J Ophthalmol.* 2011;152:256-265.
8. Hayashi K, Ohno-Matsui K, Shimada N, et al. Long-term pattern of progression of myopic maculopathy: a natural history study. *Ophthalmology.* 2010;117:1595-1611.
9. Curtin BJ. Basic science and clinical management. In: Curtin BJ, ed. *The Myopias.* New York: Harper and Row; 1985:177-202.
10. Vongphanit J, Mitchell P, Wang JJ. Prevalence and progression of myopic retinopathy in an older population. *Ophthalmology.* 2002;109:704-711.
11. Moriyama M, Ohno-Matsui K, Hayashi K, et al. Topographical analyses of shape of eyes with pathologic myopia by high-resolution three dimensional magnetic resonance imaging. *Ophthalmology.* 2011;118:1626-1637.
12. Curtin BJ. The posterior staphyloma of pathologic myopia. *Trans Am Ophthalmol Soc.* 1977;75:67-86.
13. Hogan MJ. The sclera. In: Hogan ML, Alvarado JA, Weddle JE, eds. *Histology of the Human Eye.* Philadelphia, PA: W.B. Saunders; 1971:183-201.
14. Curtin BJ, Teng CC. Scleral changes in pathological myopia. *Trans Am Acad Ophthalmol Otolaryngol.* 1958;62:777-788.
15. Curtin BJ, Iwamoto T, Renaldo DP. Normal and staphylomatous sclera of high myopia. An electron microscopic study. *Arch Ophthalmol.* 1979;97:912-915.
16. McBrien NA, Gentle A. Role of the sclera in the development and pathological complications of myopia. *Prog Retin Eye Res.* 2003;22:307-338.
17. Avetisov ES, Savitskaya NF, Vinetskaya MI, Iomdina EN. A study of biochemical and biomechanical qualities of normal and myopic eye sclera in humans of different age groups. *Metab Pediatr Syst Ophthalmol.* 1983;7:183-188.
18. McBrien NA, Cornell LM, Gentle A. Structural and ultrastructural changes to the sclera in a mammalian model of high myopia. *Invest Ophthalmol Vis Sci.* 2001;42:2179-2187.
19. Rada JA, Shelton S, Norton TT. The sclera and myopia. *Exp Eye Res.* 2006;82:185-200.
20. Funata M, Tokoro T. Scleral change in experimentally myopic monkeys. *Graefes Arch Clin Exp Ophthalmol.* 1990;228:174-179.
21. Imamura Y, Iida T, Maruko I, Zweifel SA, Spaide RF. Enhanced depth imaging optical coherence tomography of the sclera in dome-shaped macula. *Am J Ophthalmol.* 2011;151:297-302.
22. Maruko I, Iida T, Sugano Y, Oyamada H, Sekiryu T. Morphologic choroidal and scleral changes at the macula in tilted disc syndrome with staphyloma using optical coherence tomography. *Invest Ophthalmol Vis Sci.* 2011;52:8763-8768.
23. Gaucher D, Erginay A, Lecleire-Collet A, et al. Dome-shaped macula in eyes with myopic posterior staphyloma. *Am J Ophthalmol.* 2008;145:909-914.
24. Yun SH, Bouma BE. Wavelength swept lasers. In: Drexler W, Fujimoto JG, eds. *Optical Coherence Tomography: Technology and Applications.* New York, NY: Springer; 2008:359-378.
25. Ohno-Matsui K, Akiba M, Moriyama M, Ishibashi T, Hirakata A, Tokoro T. Intrachoroidal cavitation in macular area of eyes with pathologic myopia. *Am J Ophthalmol.* In press.
26. Ohno-Matsui K, Akiba M, Moriyama M, Ishibashi T, Tokoro T, Spaide RF. Imaging the retrobulbar subarachnoid space around the optic nerve by swept source optical coherence tomography in eyes with pathologic myopia. *Invest Ophthalmol Vis Sci.* 2011;52:9644-9650.
27. Spaide RF, Akiba M, Ohno-Matsui K. Evaluation of peripapillary intrachoroidal cavitation with swept source and enhanced depth imaging optical coherence tomography. *Retina.* In press.
28. Ohno-Matsui K, Akiba M, Moriyama M, et al. Acquired optic nerve and peripapillary pits in pathologic myopia. *Ophthalmology.* In press.
29. Hsiang HW, Ohno-Matsui K, Shimada N, et al. Clinical characteristics of posterior staphyloma in eyes with pathologic myopia. *Am J Ophthalmol.* 2008;146:102-110.
30. Shauly Y, Miller B, Lichtig C, Modan M, Meyer E. Tenon's capsule: ultrastructure of collagen fibrils in normals and infantile esotropia. *Invest Ophthalmol Vis Sci.* 1992;33:651-656.
31. Fujiwara T, Imamura Y, Margolis R, Slakter JS, Spaide RF. Enhanced depth imaging optical coherence tomography of the choroid in highly myopic eyes. *Am J Ophthalmol.* 2009;148: 445-450.

健康成人の片眼に発症した内因性真菌性眼内炎

宇野友絵[*1,2]　南場研一[*1]　加瀬　諭[*1]　齋藤　航[*1]　北市伸義[*3,4]　大野重昭[*4]
石田　晋[*1]

[*1]北海道大学大学院医学研究科眼科学分野　[*2]函館中央病院眼科　[*3]北海道医療大学個体差医療科学センター眼科
[*4]北海道大学大学院医学研究科炎症眼科学講座

A Case of Unilateral *Candida* Endophthalmitis in a Healthy Female

Tomoe Uno[1,2], Kenichi Namba[1], Satoru Kase[1], Wataru Saito[1], Nobuyoshi Kitaichi[3,4], Shigeaki Ohno[4] and Susumu Ishida[1]

[1]*Department of Ophthalmology, Hokkaido University Graduate School of Medicine,* [2]*Department of Ophthalmology, Hakodate Central General Hospital,* [3]*Department of Ophthalmology, Health Sciences University of Hokkaido,* [4]*Department of Ocular Inflammation and Immunology, Hokkaido University Graduate School of Medicine*

目的：健康成人に発症した片眼性真菌性眼内炎の1例について報告する．**症例**：69歳，女性．眼および全身に既往歴はない．初診時の視力は右眼0.9で，右眼に線維素析出を伴う前房炎症および一部塊状の硝子体混濁がみられた．ステロイド薬の局所治療を行ったが，強膜充血，前房蓄膿の形成，硝子体混濁の増強および斑状網膜滲出斑が出現した．ステロイド薬全身投与後にさらに増悪したため，硝子体切除術を施行した．硝子体液の培養および血清中β-D-グルカンは陰性であったが，硝子体液中のβ-D-グルカン濃度は711.6 pg/m*l*と高値を示し，硝子体細胞診のperiodic acid Schiff（PAS）染色で多数のカンジダ菌糸が確認された．**結論**：非典型的な内因性真菌性眼内炎の診断には，血中だけではなく，硝子体液中のβ-D-グルカン測定や切除検体の組織学的検査が有用である．

Purpose：To report a case of unilateral fungal endophthalmitis in a healthy female. **Case**：A 69-year-old healthy female with conjunctival redness and ocular pain of 6 days' duration in her right eye was seen at an eye clinic. Since corticosteroid eyedrops had no effect, she was referred to the Department of Ophthalmology, Hokkaido University Hospital at one month after onset of symptoms. History of ocular trauma or surgery was never reported. Severe anterior uveitis with fibrin and posterior synechia, and vitreous haze were observed in her right eye. Visual acuity was 0.9, right eye. Despite treatment with local and systemic corticosteroids, the ocular inflammation and vitreous haze gradually worsened. Chest and body X-ray, and blood test results were normal. Serum β-D-glucan was negative. Six months later, vitrectomy was performed on her right eye. The β-D-glucan value was elevated to 711.6 pg/m*l* in the vitreous fluid. Vitreous cytology disclosed *Candida* with periodic acid-Schiff staining. **Conclusion**：In diagnosing atypical fungal endophthalmitis, vitreous fluid β-D-glucan determination and vitreous cytology are usuful.

〔Atarashii Ganka (Journal of the Eye) **29**(1)：135～138, 2012〕

Key words：真菌性眼内炎，β-D-グルカン，硝子体手術，カンジダ，periodic acid Schiff（PAS）染色．fungal endophthalmitis, β-D-glucan, vitrectomy, *Candida*, periodic acid-Schiff stain (PAS stain).

はじめに

内因性真菌性眼内炎は経中心静脈内高カロリー輸液（intravenous hyperalimentation：IVH）留置，または悪性腫瘍，臓器移植後，あるいは免疫抑制薬の長期投与など，免疫能の低下を招く基礎疾患を背景に発症することが広く知られている．約78%が両眼性発症であり[1]，片眼性は少ない．今回筆者らは，上述する発症因子のみられない健康成人の片眼に発症し，診断・治療に苦慮したが，最終的に硝子体手術検体の鏡検で確定診断がついた真菌性眼内炎の1例を経験したので報告する．

〔別刷請求先〕宇野友絵：〒060-8638 札幌市北区北15条7丁目　北海道大学大学院医学研究科眼科学分野
Reprint requests：*Tomoe Uno, M.D., Department of Ophthalmology, Hokkaido University Graduate School of Medicine, Kita 15, Nishi 7, Kita-ku, Sapporo 060-8638, JAPAN*

0910-1810/12/¥100/頁/JCOPY

I 症　　例

患者：69歳，女性．

主訴：右眼充血，眼痛．

現病歴：2008年7月19日右眼に充血，眼痛が出現した．改善がみられないため7月25日近医を初診した．右眼に線維素析出，虹彩後癒着を伴う前房炎症がみられ，ステロイド薬の点眼治療で改善がみられないため，発症から約1カ月後の8月18日に北海道大学病院眼科を紹介され初診した．

既往歴：1998年に大腸癌で大腸部分切除術を受けているが，その後再発や転移はみられていない．内眼手術や眼外傷の既往はない．

初診時眼所見：視力は右眼0.9（矯正不能），左眼0.3（0.8×+1.25D），眼圧は右眼14mmHg，左眼21mmHgであった．右眼に線維素析出，虹彩後癒着を伴う前房炎症，そしてびまん性，一部塊状の硝子体混濁がみられた（図1）．一方，網膜滲出斑，出血，網膜血管の白鞘化はみられなかった．また，左眼に異常はみられなかった．

検査所見：血液検査，尿検査では血清β-D-グルカンを含め異常はみられず，胸部X線写真でも異常所見はなかった．加えて全身的に真菌感染症を疑う所見はなく，この時点でぶどう膜炎の原因同定には至らなかった．

経過：2008年8月から2009年2月までの経過を図2に示す．初診時からステロイド薬の点眼治療のみで経過をみていたが，前房炎症・硝子体混濁は持続した．炎症悪化時にはデキサメタゾン結膜下注射やトリアムシノロンアセトニド後部Tenon嚢下注射を適宜施行したが，反応は乏しかった．

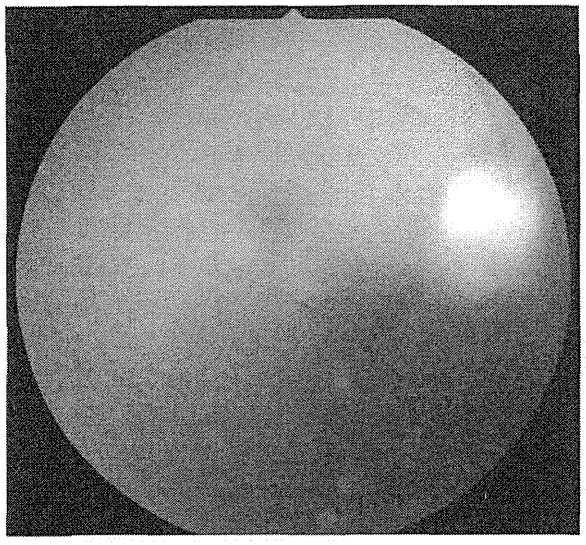

図1　初診時の右眼眼底写真
びまん性および一部塊状の硝子体混濁がみられる．

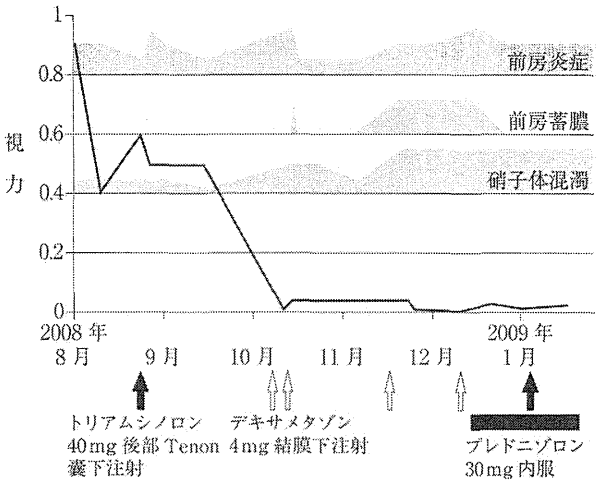

図2　2008年8月から2009年2月までの右眼視力と炎症所見の推移

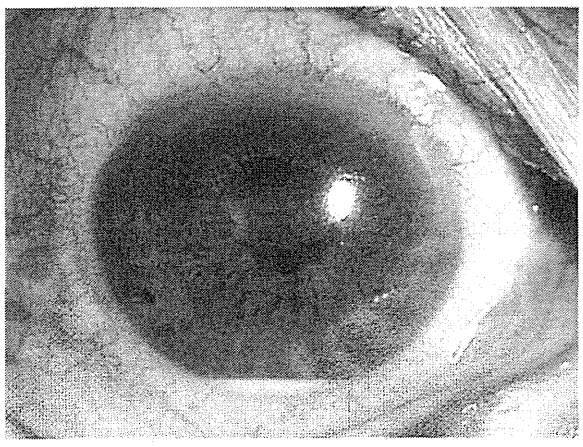

図3　2008年10月時の右眼前眼部写真
右眼視力は0.01（矯正不能）に低下し，強い強膜充血と前房蓄膿の形成がみられる．

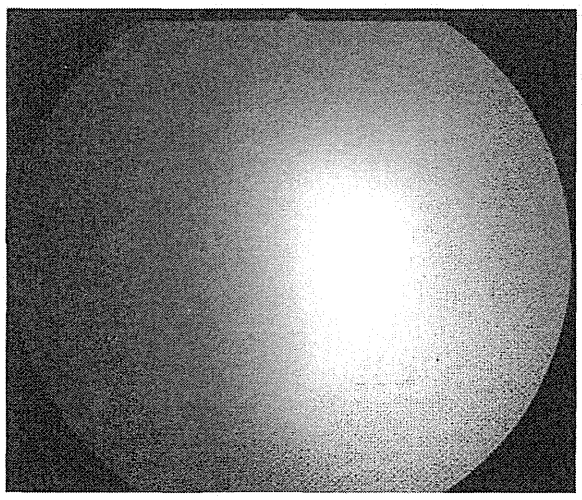

図4　2009年2月時の右眼眼底写真
硝子体混濁は増悪し雪土手状滲出性病変が出現している．

2008年10月右眼炎症所見が増悪し，右眼矯正視力は0.01に低下した．強膜充血，前房蓄膿の形成（図3），硝子体混濁の増強および斑状網膜滲出斑が出現した．プレドニゾロン内服を開始したが右眼炎症所見は改善しなかった．その後，耳側網膜周辺部に円周状の白色混濁が集積した雪土手状滲出性病変が出現し，硝子体混濁も増悪した（図4）．再び原因検索のため，前房水を採取してpolymerase chain reaction（PCR）検査を行ったが，水痘帯状ヘルペスウイルス，単純ヘルペスウイルス，サイトメガロウイルスのいずれのDNAも検出されなかった．血液中のβ-D-グルカン値，カンジダ抗原，トキソカラ抗体（enzyme-linked immunosorbent assay：ELISA法）検査もいずれも陰性であった．この時点で診断的硝子体手術を考慮したが患者の同意が得られなかった．積極的に感染症を疑う根拠に乏しく，炎症性疾患を考えてステロイド薬治療を継続し，改善・悪化がみられず経過した．しかし，ステロイド薬への反応が乏しいこと，病状の進行が比較的緩やかであること，雪土手状滲出性病変の存在から真菌性眼内炎を疑い，2009年2月19日から抗真菌薬（ミカファンギン）の点滴を開始し，2月22日，患者の同意が得られたため右眼硝子体切除術を施行した．採取された硝子体液の培養検査では菌の発育はなかったが，硝子体液中のβ-D-グルカンの濃度は711.6 pg/mlと高値を示した．また，硝子体細胞診のperiodic acid Schiff（PAS）染色標本に多数のカンジダ菌糸が確認され（図5），真菌性眼内炎と診断した．手術翌日の2月23日からボリコナゾール点滴に変更したが，3月2日に右眼は網膜全剝離に至り，3月3日に再度硝子体手術を行った．術中，網膜の全面にわたって線維血管増殖膜形成を伴う網膜剝離がみられたため，増殖膜を除去しシリコーンオイルタンポナーデを行った．その後再剝離したが，患者は積極的治療を望まないため，経過を観察している．ボリコナゾール投与は38日間行い，前房，硝子体中の炎症所見は消失した．現在，右眼視力は眼前手動弁で炎症の再燃はない．

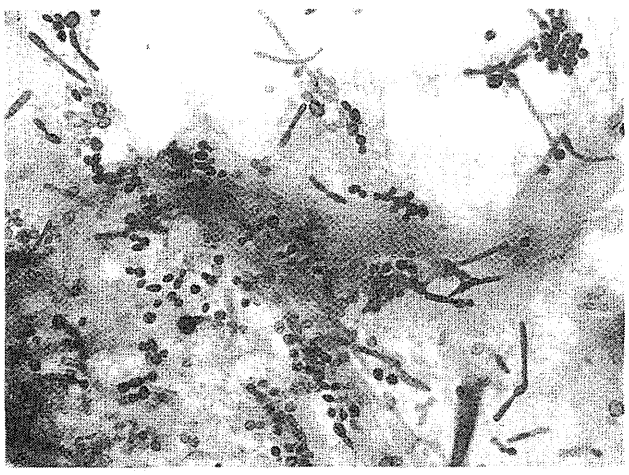

図5　硝子体液のPAS染色標本
PAS陽性のカンジダ菌糸が多数検出された．

II　考　　按

健康成人の片眼に発症した非典型的な内因性真菌性眼内炎の1例を経験した．内因性真菌性眼内炎は，通常IVH留置や免疫低下を招く基礎疾患を背景に血行性に発症する．診断の確定には，前房水あるいは硝子体液からの真菌の検出が必要であるが，実際に眼内組織から真菌が分離，培養される頻度は30～50%と低い[2~5]．一方，一般的に他臓器もしくは全身性の真菌感染症が先行するため血中β-D-グルカン値の測定が診断に有用である．実際Takebayashiら[1]は，真菌性眼内炎における血中β-D-グルカンの陽性率は95%と報告しており，感度の高い検査といえる．

しかしながら，本症例のように血中β-D-グルカンの上昇を伴わない内因性真菌性眼内炎の報告もある．表1に示すように，健康成人に発症した内因性真菌性眼内炎は本症例を含めて9例[6~11]報告されている．Schmidらの報告[6]では，片眼，両眼の記載がなく詳細は不明であるが，その他の報告では7例のうち6例が片眼性であり，健康成人に発症する真菌性眼内炎は片眼性が多い．また，藤井ら[10]や岩瀬ら[11]の報告例，および本症例では血中β-D-グルカンは陰性であった．したがって片眼性の症例では，外因性の真菌感染を疑う必要があるが，本症例では内眼手術および眼外傷の既往がなく，

表1　健康成人に発症した真菌性眼内炎の報告

	症例数	片眼or両眼	血中β-D-グルカン	硝子体液中β-D-グルカン	文　献
Schmidら	2例	不明	（培養のみ）	（培養のみ）	Infection, 1991[6]
Kostickら	1例	片眼	（培養のみ）	（培養のみ）	Am J Ophthalmol, 1992[7]
酒井ら	2例	片眼 片眼	（培養のみ） （培養のみ）	（培養のみ） （培養のみ）	臨眼，1997[8]
板野ら	1例	片眼	＋	＋	眼臨，2006[9]
藤井ら	1例	片眼	－	＋	臨眼，2009[10]
岩瀬ら	1例	両眼	－	＋	あたらしい眼科，2010[11]
本症例	1例	片眼	－	＋	

角膜，結膜，強膜，虹彩，水晶体に外傷の痕跡はなかった．

最近，硝子体液中のβ-D-グルカンが真菌性眼内炎の診断に有用であることが示唆されている．真保ら[12]は真菌性眼内炎2例を含む26症例について硝子体液中のβ-D-グルカン値を測定し，硝子体液中β-D-グルカンの基準値は10.0 pg/ml以下とした．β-D-グルカン値の測定は培養検査よりも真菌に対して感度が高く簡便であるため，真菌性眼内炎の診断をするうえでの適切な指標となりうると報告している[7]．

前述した健康成人に発症した真菌性眼内炎の報告のなかで，硝子体液中のβ-D-グルカンの測定値についても記載があり，板野らの報告[9]では血中および硝子体液中のβ-D-グルカンがともに陽性であった（表1）．一方，藤井らや岩瀬らの報告および本症例では血中β-D-グルカンは陰性であるが硝子体液中のβ-D-グルカンは陽性を示しており，血中よりも有用であることが示唆される．したがって，真菌感染症を疑わせる背景のない患者で眼所見から内因性真菌性眼内炎が疑われる場合や，外因性（外傷，術後）眼内炎で真菌が原因である可能性がある場合には，硝子体液中β-D-グルカン値の測定が有用であると考えられる．

一般に内因性真菌性眼内炎は血行感染であり，結果として両眼性が多いが，健康成人の片眼に発症する真菌性眼内炎は一般的な真菌性眼内炎とは発症経路が異なる可能性が考えられる．Kostickらの報告[7]では，片眼の真菌性眼内炎を発症した健康成人の膣および爪からカンジダが検出されており，その発症となんらかの関連があることが示唆されている．しかし，その感染経路の詳細については言及されていない．本症例でも感染経路の特定はできなかった．

本症例は真菌性眼内炎に特徴的な発症因子がなく，血清β-D-グルカンが陰性であったこと，加えて本人が手術に消極的であったことが真菌性眼内炎の診断が遅れる結果となった．真菌の侵入経路はいまだに不明であるが，内因性真菌性眼内炎が健康成人の片眼に生じうる可能性を認識しておくべきである．眼所見から真菌性眼内炎が疑われる症例では積極的に硝子体切除術を行い，眼内液の培養以外にも硝子体液中β-D-グルカンの測定，硝子体液の細胞診を行うことが大切である．

文　献

1) Takebayashi H, Mizota A, Tanaka M：Relation between stage of endogenous fungal endophthalmitis and prognosis. *Graefes Arch Clin Exp Ophthalmol* **244**：816-820, 2006
2) 秦野　寛，井上克洋，的場博子ほか：日本の眼内炎の現状．日眼会誌 **95**：369-376, 1991
3) 金子尚生，宮村直孝，沢田達宏ほか：内因性眼内炎の予後．眼紀 **44**：469-474, 1993
4) 川添真理子，沖波　聡，齊藤伊三雄ほか：内因性真菌性眼内炎に対する硝子体手術．臨眼 **48**：753-757, 1994
5) 久保佳明，水谷　聡，岩城正佳ほか：真菌性眼内炎の硝子体手術による治療．臨眼 **48**：1867-1872, 1994
6) Schmid S, Martenet AC, Oelz O：Candida endophthalmitis：Clinical presentation, treatment and outcome in 23 patients. *Infection* **19**：21-24, 1991
7) Kostick DA, Foster RE, Lowder CY et al：Endogenous endophthalmitis caused by Candida albicans in a healthy woman. *Am J Ophthalmol* **113**：593-595, 1992
8) 酒井理恵子，川島秀俊，釜田恵子ほか：健常者に発症した真菌性眼内炎の2症例．臨眼 **51**：1733-1737, 1997
9) 板野瑞穂，植木麻理，岡田康平ほか：血中β-D-グルカン測定が診断に有用であった健常者発症真菌性眼内炎の1例．眼臨 **100**：758-760, 2006
10) 藤井　澄，岡野内俊雄：硝子体液中β-D-グルカンおよび真菌PCRが眼内炎の診断・治療に有用であった1例．臨眼 **63**：69-73, 2009
11) 岩瀬由紀，竹内　聡，竹内正樹ほか：健康な女性に発症した両眼性の真菌性眼内炎の1例．あたらしい眼科 **27**：675-678, 2010
12) 真保雅乃，伊藤典彦，門之園一明ほか：硝子体液中β-D-グルカン値の臨床的意義の検討．日眼会誌 **106**：579-582, 2002

*　　*　　*